Q. J. R. Meteorol. Soc. (1998), **124**, pp. 2393–2415

Correction for attenuation of radar reflectivity using polarization data

By T. J. SMYTH* and A. J. ILLINGWORTH
University of Reading, UK

(Received 4 September 1997; revised 11 May 1998)

SUMMARY

Attenuation by heavy rain is a major operational problem in radar estimation of rainfall rates, and one which is increasingly severe at wavelengths shorter than 10 cm. Gate-by-gate correction algorithms, including those using both reflectivity (Z_H) and differential reflectivity (Z_{DR}), are inherently unstable. In addition values of Z_H and Z_{DR} are affected by hail, which causes little attenuation. Methods dependent upon differential phase shift (K_{DP}) do not give unique solutions but depend upon raindrop size distributions. A new technique which uses both K_{DP} and differential attenuation between the horizontally and vertically polarized radiation (A_{H-V}) is proposed. The total A_{H-V} is measured from the negative Z_{DR} in light precipitation behind the attenuating region. Theory and observation show that corrections based on the $K_{DP} - A_{H-V}$ scheme should be unaffected by hail, stable and accurate. A simpler algorithm may be feasible at C-band in which the total attenuation is derived from the observed total differential attenuation. It appears that the most severe cases of attenuation result from heavy rain consisting of large oblate raindrops. Accordingly, the attenuation would be appreciably reduced if operational radars used vertical polarization rather than the commonly employed horizontal polarization.

KEYWORDS: Heavy rain Rainfall estimation Vertical polarization

1. INTRODUCTION

If reliable rainfall rates for regions of intense precipitation are to be calculated using radar, then correction for attenuation is necessary. Attenuation becomes increasingly more serious as the wavelength, λ, is reduced. At S-band ($\lambda = 10$ cm) the effect has previously been considered to be negligible (Hitschfeld and Bordan 1954), whereas C-band ($\lambda = 5$ cm; the wavelength of many operational radars in Europe) attenuation due to precipitation is well known to disrupt rainfall rate estimation. The gate-by-gate attenuation correction scheme of Hitschfeld and Bordan (1954) which relies on a relationship between attenuation, A, and reflectivity, Z, is known to be very unstable and, as shown by Hildebrand (1978), extremely sensitive to calibration errors. Delrieu *et al.* (1991) have computed relationships between A and Z for different wavelengths, temperatures and drop size distributions (DSDs) assuming the raindrops to be spherical. They show that at C-band the attenuation at 20 °C is typically about 75% of the value at 0 °C and, for example, that for a 100 mm hr^{-1} rainfall rate and 0 °C they predict that different DSDs can give one-way attenuations ranging from 0.43 to 0.67 dB km^{-1}. For airborne radar the 'stereoradar' technique (Kabeche and Testud 1995) relies on observing precipitation cells from two angles. A very simple version of this technique could be used when two neighbouring radars in a network provide overlapping coverage; it is most unlikely that the paths from both radars will suffer attenuation, so only the unaffected beam is used. However, for most operational networks such overlapping regions are not widespread. Recently, Delrieu *et al.* (1997) reported a ground-based version of the 'surface reference technique' developed for spaceborne radars. This method, using an X-band radar in mountainous terrain, relies on measuring the reflectivity of a well-defined distant clutter target when there is attenuation to estimate the path integrated attenuation, and then using this as a constraint for the gate-by-gate retrieval. Such a technique may be appropriate at X-band where attenuation is very severe, but the accuracy is limited, for example, by the day-to-day variation of about 3 dBZ in the apparent reflectivity of the clutter target in dry weather.

* Corresponding author, present address: Plymouth Marine Laboratory, Prospect Place, Plymouth, Devon PL1 3DH, UK. e-mail: T.J.Smyth@pml.ac.uk.

This paper presents observations of a severe convective event on 7 June 1996, which caused severe differential attenuation (A_{H-V}) between the horizontally polarized (A_H) and vertically polarized (A_V) copolar returns of up to 5 dB, by the S-band Chilbolton multi-parameter radar in southern England. Rapid-response raingauges, situated 500 m below the precipitation region causing the radar attenuation, measured values in excess of 250 mm hr^{-1}. A numerically stable algorithm to correct for reflectivities measured with horizontal and vertical polarizations is proposed which relies on both A_{H-V} and differential phase shift (ϕ_{DP}).

2. Definition of radar parameters

Differential reflectivity is defined as (Seliga and Bringi 1976):

$$Z_{DR} = 10 \log_{10} \frac{Z_H}{Z_V} \quad \text{(dB)}, \tag{1}$$

where Z_H and Z_V are the backscattered reflectivity in the horizontal and vertical polarizations respectively. Z_{DR} is a measure of the reflectivity-weighted oblateness (Jameson 1983). Raindrops are oblate to a degree which increases with size, and fall with their minor axis oriented vertically. Rain can therefore be described as an anisotropic medium. High positive values of Z_{DR} are associated with large oblate raindrops.

The one way absolute attenuation, using the formulation of Oguchi (1973), is defined as:

$$A_H = 8.686 \times 10^3 \lambda \int \mathrm{Im}[S_{fH}(D_e)] N(D_e)\, dD_e \quad \text{(dB km}^{-1}\text{)}, \tag{2}$$

where D_e is the spheroid equivolumetric diameter of the drops, $\mathrm{Im}(S_{fH}(D_e))$ (m) is the imaginary component of the forward-scatter amplitude in the horizontal polarization and N is the number of particles per unit size per unit volume. When dual polarization radar illuminates a region filled with oblate spheroids oriented with their minor axes vertical, such as in rain, the horizontal polarization will become attenuated to a greater extent than the vertical. This differential attenuation is defined as:

$$A_{H-V} = 8.686 \times 10^3 \lambda \int \mathrm{Im}[S_{fH}(D_e) - S_{fV}(D_e)] N(D_e)\, dD_e \quad \text{(dB km}^{-1}\text{)}, \tag{3}$$

where S_{fV} is the forward-scattering amplitude (m) for vertically polarized waves. A factor of two is required in (2) and (3) to account for two-way attenuation. A_{H-V} can be deduced by the magnitude of negative Z_{DR} in light precipitation behind an attenuating region. In these regions Z_{DR} should be close to zero as the raindrops will be approximately spherical. For example, if Z_{DR} is -2 dB in light rain then the total path integrated A_{H-V} along the ray is 2 dB.

The differential phase shift, ϕ_{DP}, is the difference in phase between the copolar radar returns measured with vertical and horizontal polarization ($\phi_V - \phi_H$). ϕ_{DP} is made up of three contributions: a propagation component (K_{DP}), which is a function of range, differential phase shift on backscatter (δ) and a hardware offset (ϕ_o). i.e.

$$\phi_{DP}(r) = 2 \int_0^r K_{DP}(r)\, dr + \delta(r) + \phi_o \quad (^\circ), \tag{4}$$

where r is the range. K_{DP} is defined as:

$$K_{DP} = 2 \times \frac{180 \times 10^3 \lambda}{\pi} \int \mathrm{Re}[S_{fH}(D_e) - S_{fV}(D_e)] N(D_e)\, dD_e \quad (^\circ \text{ km}^{-1}). \tag{5}$$

The factor of two is for two-way propagational differential phase shift, and the factor of 10^3 is a conversion from $^\circ$ m^{-1} to $^\circ$ km^{-1}. As the incident wave propagates through a region of rain the horizontally polarized wave lags progressively behind the vertical one, because raindrops display a high degree of anisotropy. This causes a positive differential phase shift. In rain the value of K_{DP} is approximately proportional to the rain-rate, R. A relationship of the form:

$$K_{DP} = 0.03R^{1.15} \quad (^\circ \text{ km}^{-1}) \tag{6}$$

at S-band has been proposed by Sachidananda and Zrnić (1986). At S-band δ is usually considered to be very small, as it only occurs in the Mie regime, that is for raindrops of size 7 mm and rather larger for dry hailstones; it is only measurable if the hydrometeors have a preferred orientation (McCormick *et al.* 1979), not if randomly oriented. It is important to note that δ, being a backscatter effect, is a transitory change in ϕ_{DP} superposed on the general propagation effect, and can introduce ambiguity in the interpretation of the signal. The observed δ for a distribution of scatterers in the pulse volume can be calculated using the cross correlation coefficient ρ_{HV}:

$$\rho_{HV} = \frac{\int S_{bH}(D_e) S^*_{bV}(D_e) N(D_e)\, dD_e}{[\int |S_{bH}|^2 N(D_e)\, dD_e]^{1/2} [\int |S_{bV}|^2 N(D_e)\, dD_e]^{1/2}}, \tag{7}$$

$$\rho_{HV} = |\rho_{HV}| \exp(j\delta), \tag{8}$$

where S_{bH} and S_{bV} are the backscatter amplitudes in the horizontal and vertical, and the units of δ are radians.

3. Attenuation correction algorithms

(a) *Single parameter*

Several attenuation correction algorithms have been derived and implemented on both actual and simulated data. The simplest algorithms involve the use of reflectivity-only (Z-only) data (see e.g. Hitschfeld and Bordan (1954) and Hildebrand (1978)), are generally gate-by-gate iterative schemes and prove to be highly numerically unstable. The UK Meteorological Office (UKMO) attenuation correction scheme is a cumulative gate-by-gate algorithm of the form:

$$A = 0.0044R^{1.17} \quad (\text{dB km}^{-1}), \tag{9}$$

for the two way attenuation (Collier 1990) based on the work of Gunn and East (1954). This procedure is prone to instability and so the predicted correction is capped; the maximum correction factor allowed is a doubling of the rainfall. This is being used operationally for all UK radars from 1998 and is similar to that in use in Sweden and Spain (A. Smith, UKMO, personal communication). A great deal of the instability in single-parameter schemes is caused by initial radar calibration (Hitschfeld and Bordan 1954). Z only schemes are also unable to distinguish between rain and hail (because $Z \propto D^6$, where D is the particle diameter, and contains no information about the composition of the precipitation volume) which could lead to spurious amounts of correction via the conversion to rain rate.

(b) *Dual parameter*

Aydin *et al.* (1989) formulated a theoretical correction algorithm for use at C-band using a combination of Z_H and Z_{DR}. From the premise that R estimates are improved by using the Z_H and Z_{DR} pair, it is a natural progression to the assumption that the introduction of Z_{DR} should improve estimates of attenuation. Using DSDs obtained by distrometer

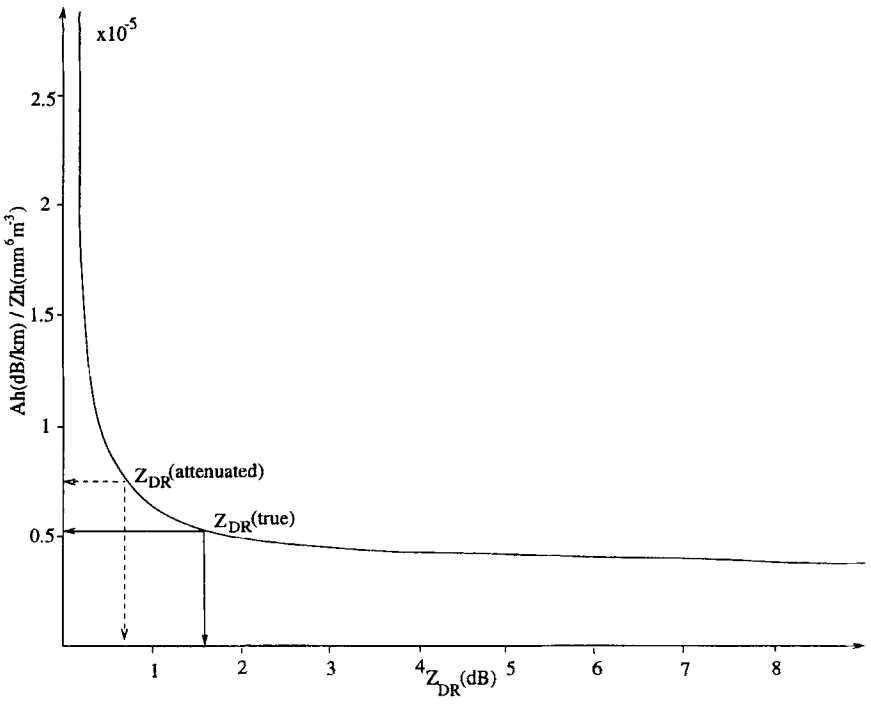

Figure 1. Differential reflectivity, Z_{DR}, against the ratio of horizontally polarized attenuation to backscattered reflectivity, A_H/Z_H. This shows the compensation effect at C-band using Beard and Chuang (1987) shapes and Marshall–Palmer drop size distribution at $T = 0$ °C. See text for further explanation.

measurements, they modelled backscattering and extinction cross-sections to obtain the radar parameters of Z_H, Z_{DR}, and calculated A_H and A_{H-V}. They derived empirical relationships between A_H or A_V and the Z_H, Z_{DR} pair using a least squares polynomial fit. A gate-by-gate scheme was employed to produce a first-order correction, and an iteration process invoked at the nth gate which was repeated until the absolute difference between two consecutive approximations of Z_H and Z_{DR} at that gate were less than 0.1 dBZ and 0.05 dB respectively. They found, however, that those conditions were satisfied within one iteration. To test for noise and biases they simulated radar data, and found that any bias in Z_H deteriorated that procedure because the errors add cumulatively. Scarchilli *et al.* (1993) used a similar scheme but they parametrized A_H and A_{H-V} in terms of Z_H and Z_{DR}.

Tan and Goddard (1997) describe a scheme which does not rely upon a gate-by-gate iterative technique and is therefore highly numerically stable. Instead, a compensation method is used, which employs relationships between A_H, A_V and the Z_H, Z_{DR} pair. This is illustrated in Fig. 1, and relies on the negative slope of the A_H/Z_H against Z_{DR} curve. The effect of attenuation will be to reduce the observed values of both Z_H and Z_{DR}. If the attenuated value of Z_{DR} is used, rather than the true value, then the negative value of the slope in Fig. 1 means that the computed value of A_H/Z_H is larger than it should be. However, if when evaluating A_H/Z_H we use the observed attenuated value of Z_H, then the resultant predicted value of A_H will be close to the true one. The errors caused by using the attenuated values of both Z_H and Z_{DR} thus tend to cancel out, and the calculated value of A_H is closer to the true one than if Z_H alone is used.

The technique, then, is to use the uncorrected values of Z_H and Z_{DR}, and to predict a value of A_H at each gate. This value of A_H is then used at each gate to correct Z_H on a gate-by-gate basis. When Z_{DR} becomes very small the scheme is difficult to implement because of the increasingly steep slope of the curve in Fig. 1. If the attenuation is so large that Z_{DR} becomes negative then an alternative approach is needed. Tan and Goddard (1997) suggest using a relationship between A_H and A_{H-V}:

$$A_{H-V} = A_H - A_V \quad (\text{dB km}^{-1}), \tag{10}$$

$$A_H \simeq 2.95 \times A_{H-V} + 0.084 \quad (\text{dB km}^{-1}), \tag{11}$$

this relationship being empirical and unique to C-band. An iterative step is invoked if any negative values of Z_{DR} remain.

The fundamental difficulty with all $Z_H - Z_{DR}$ schemes is the assumption that only rain is present. When hail occurs Z_H increases and Z_{DR} falls, and such schemes will erroneously infer exceptionally heavy rain consisting of small drops, with consequently spurious high levels of attenuation.

(c) *Differential phase scheme*

ϕ_{DP} is ideally suited for use in an attenuation correction algorithm, because it has similar features to A_H and A_{H-V}. Both are forward-scatter effects; the real part of the forward-scatter amplitudes is proportional to K_{DP} whereas the imaginary part is proportional to attenuation. ϕ_{DP} itself is not affected by attenuation as it measures the difference in phase, and it is also relatively unaffected by hail. An additional factor is that raindrops become more oblate with increasing size, implying that K_{DP} increases with increased specific differential attenuation which implies that there is some form of relationship between the two parameters.

The use of ϕ_{DP} to correct for attenuation was first suggested by Bringi *et al.* (1990) and their calculations have been re-worked in section 5. They suggested the use of linear relationships between K_{DP} and both A_H and A_{H-V}. As will be shown in section 5, the use of a single linear relationship is equivalent to assuming a constant value of the median DSD diameter, D_0 (mm), but allowing the concentration of drops, N_0 ($\text{m}^{-3}\text{mm}^{-1}$), to vary in the standard exponential rain DSD e.g.

$$N(D) = N_0 \exp\left(\frac{-3.67 \times D}{D_0}\right) \quad \text{m}^{-3}\text{mm}^{-1}, \tag{12}$$

where N_0 is the intercept of the curve on the N axis. In their simulations Bringi *et al.* (1990) did not allow D_0 to rise above 2.5 mm, a very low value for heavy precipitation.

4. Observations

In this paper we propose a method of correcting for attenuation which involves *both* differential phase shift and the accumulated differential attenuation (i.e. negative Z_{DR} on the far side of the storm). An example is shown in Fig. 2 where the differential attenuation and differential phase shift are clearly visible behind shafts of heavy rain. The 'stripes' of negative Z_{DR} and phase shift emanate from a region behind an intense rainfall shaft (where Z_{DR} is > 4 dB) in a manner analogous to a shadow, pointing to the region where attenuation is occurring. Two regions of A_{H-V} are apparent from Fig. 2 along radials of 270° and 240°. Also shown in Fig. 2 are the positions of two rapid-response drop counting gauges (g5 and g7) which provided 30-second resolved rain rate estimates.

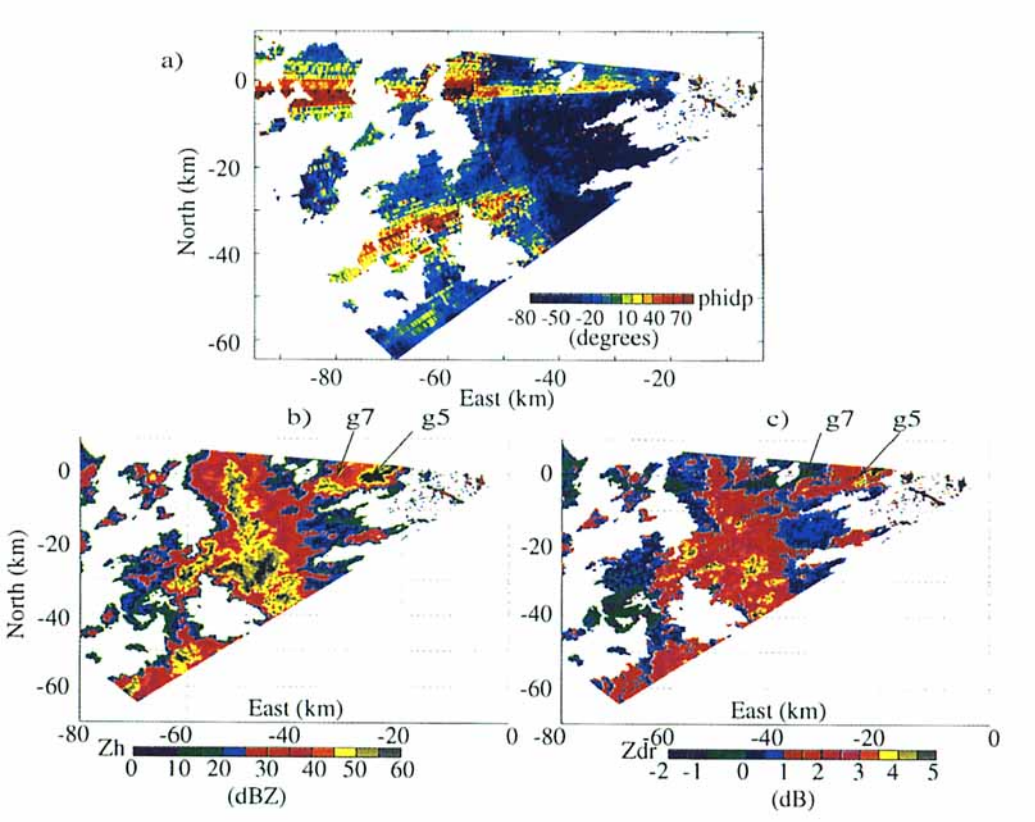

Figure 2. Plan position indicator of (a) differential phase shift, ϕ_{DP}, (b) backscatter reflectivity, Z_H and (c) differential reflectivity, Z_{DR} at 1936:09 UTC 7 June 1996; g5 and g7 are raingauge positions.

Ryzhkov and Zrnić (1994) draw attention to the existence of differential attenuation accompanying large values of differential phase shift. Although the ray profile they show is very noisy, with 50° noise on ϕ_{DP} and 1 dB on Z_{DR}, they present a statistical analysis suggesting the amount of A_{H-V} for a given ϕ_{DP} is about twice as much as predicted by Bringi *et al.* (1990).

5. Scattering calculations

(*a*) *Hail*

The scattering coefficients for hailstones of various structural compositions, i.e. dry, spongy (30% water-ice mixture) or covered with a layer of water, were extracted using the T–matrix code (Waterman 1965), and the effect of shape and alignment investigated. The dielectric constants for water and ice were those calculated by Ray (1972) and Liebe *et al.* (1989). Dry hail (hail above the melting layer) was modelled using the dielectric constant of dry ice ($3.15 + 0.0004i$; at 0 °C and $\lambda = 9.75$ cm). In all cases there is no air contained in the mixture. Spongy hail contains water within a frozen ice lattice and can be considered to be a homogeneous mixture of the two; the dielectric constant can be extracted using the Bruggemann rule (O'Brien and Geodecke 1988). Wet hail was modelled using both

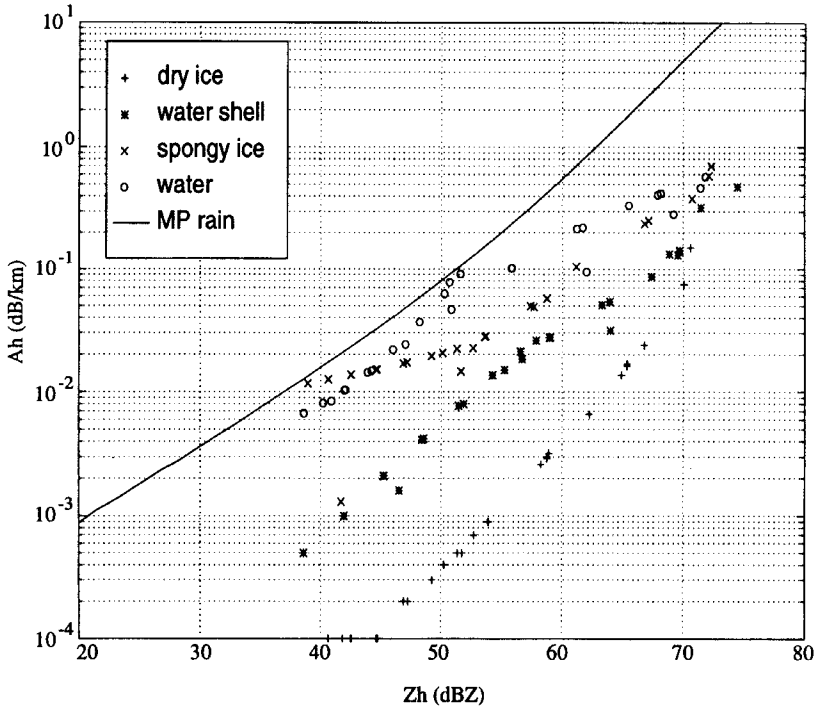

Figure 3. S-band comparison of horizontally polarized backscatter reflectivity, Z_H against attenuation, A_H, for hail varieties and Marshal–Palmer drop size distribution (MP) rain at 0 °C. γ from (13) is varied between 0.1 and 2 mm^{-1} for all hailstone compositions. See text for further explanation.

the dielectric constant of water (79.082 + 25.351i; at 0 °C and $\lambda = 9.75$ cm) and using two-layer calculations which essentially considered a central ice core embedded within a water shell 0.01 cm thick (Atlas *et al.* 1960).

The concentration of the hailstones was modelled using the exponential DSD empirically derived by Cheng and English (1983):

$$N(D_e) = 115\gamma^{3.63}\, e^{-\gamma D_e} \quad (m^{-3}\ mm^{-1}), \tag{13}$$

where D_e is in mm. Using the hail data, Cheng and English found that γ did not fall outside the range of 0.1–2.0 mm^{-1}.

Figure 3 shows a comparison between the amounts of A_H resulting from spherical hailstones, and Marshall and Palmer (1948; MP; $N_0 = 8000\ m^{-3}\ mm^{-1}$ in (12)) rainfall. The hail data points in Fig. 3 refer to the different physical compositions. Within each physical category γ in (13) is varied between 0.1 and 2.0 mm^{-1}. These calculations, which are displayed in Fig. 3, suggest that at S-band most attenuation is produced when $Z_H > 60$ dBZ, and that the hail contributes very little to the attenuation because it is present in such low concentrations. Because of these low concentrations, the K_{DP} of hail is much less than that of rain even if it is wet, aligned and oblate.

(*b*) *Rain*

To model the effect of rain, a normalised gamma DSD (14) was used (Blackman 1996) in preference to the gamma DSD and its associated relationships proposed by Ulbrich

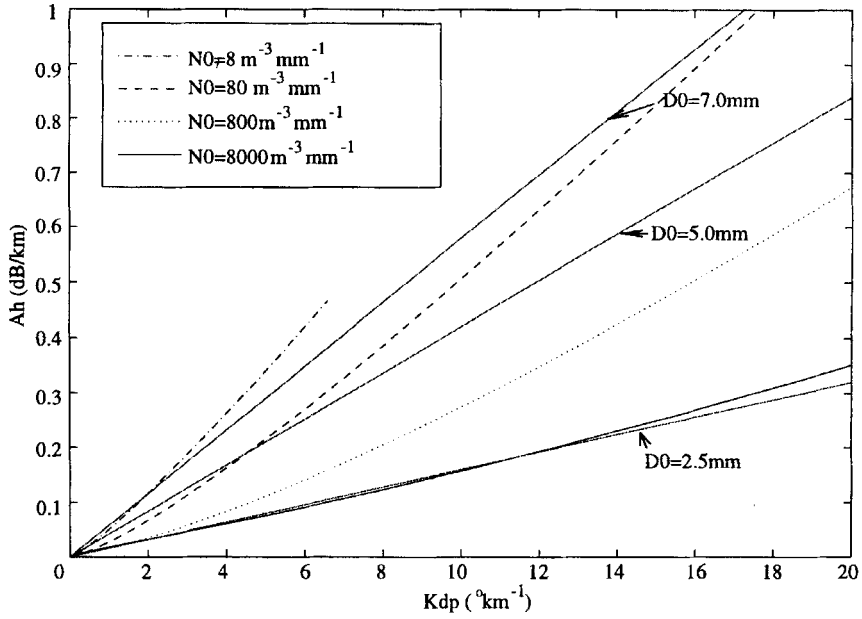

Figure 4. S-band propagation, K_{DP}, as a function of attenuation, A_H, using Beard and Chuang (1987) shapes at 20°C, with various values of raindrop concentration, N_0, in the drop size distribution ($\mu = 0$). The $N_0 = 8$ m^{-3} mm^{-1} line is shorter as all the data points for equivolumetric diameters, D_0, varying between 0 and 10 mm are contained within the axis bounds.

(1983):

$$N(D_e)\,dD_e = \frac{N_0}{|\mu|!}(\Gamma D_e)^{\mu}\,e^{-\Gamma D_e}\,dD_e \quad (m^{-3}), \tag{14}$$

and

$$\Gamma = \frac{(3.67+\mu)}{D_0} \quad (mm^{-1}), \tag{15}$$

where μ describes the form of the distribution. Studies using radar have found μ to vary between 0 and 5 (Wilson *et al.* 1997), and 2 and 4 (Illingworth and Caylor 1989). A distrometer study by Goddard and Cherry (1984) showed μ to be closer to 5. In this paper, to obtain the variability found in naturally occurring rain, we vary μ between 0 and 5 in the normalised gamma DSD of (14). The shapes of Beard and Chuang (1987) were used in preference to those of Green (1975) and Pruppacher and Pitter (1971); Caylor (1989) found that Beard and Chuang shapes gave the best approximation to what was observed by the Chilbolton radar in naturally occurring rain.

Figures 4 and 5 are a re-working of Bringi *et al.* (1990) calculations of the relationships between A_H and A_{H-V} against K_{DP} for various raindrop size spectra. Bringi *et al.* considered that a D_0 of 2.5 mm was the maximum likely to occur. A D_0 of 2.5 mm is equivalent to a Z_{DR} of 3 dB, yet values of Z_{DR} up to 6 dB are observed in rain; so in Figs. 4 and 5 we have extended values of D_0 up to 7 mm and truncated the spectrum at 10 mm. (The curves plotted are for pure exponentials with $\mu = 0$.) Whereas Bringi *et al.* found a single relationship linking K_{DP} to the two attenuation coefficients, the inclusion of larger mean drop sizes leads to a family of curves predicting higher attenuation for a given K_{DP}.

K_{DP}, A_H and A_{H-V} are all proportional to N_0 (see (2), (3), and (5)), so in Figs. 4 and 5 lines of constant D_0 are straight lines through the origin, with N_0 varying along the straight

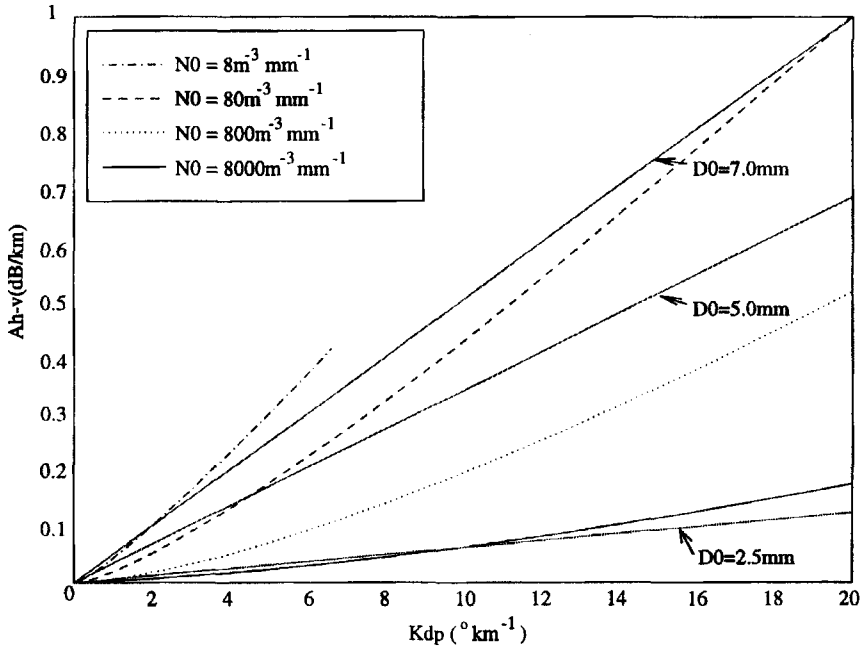

Figure 5. As Fig. 4, but K_{DP} as a function of differential attenuation, A_{H-V}.

line. The proposed single linear relationship of Bringi *et al.* between K_{DP} and both A_H and A_{H-V}, is then equivalent to assuming that in attenuating rainfall D_0 is constant and equal to 2.5 dB, and Z_{DR} (when corrected for attenuation) is constant in the rain at 3 dB.

Also shown in Fig. 4 and 5 are the lines of constant N_0 showing, for example, that the $D_0 = 7$ mm line initially intercepts the $N_0 = 8\ m^{-3}\ mm^{-1}$ and then, when $K_{DP} = 18°\ km^{-1}$, $N_0 = 80\ m^{-3}\ mm^{-1}$. The graph for $N_0 = 8\ m^{-3}\ mm^{-1}$ corresponds to a low concentration of increasingly large raindrops, and the line is terminated when the value of D_0 is so big that the rainfall rate becomes unrealistically large. Because the spectra are truncated at 10 mm these high D_0 spectra are effectively almost monodispersed, containing only very large raindrops. It needs to be noted that the relationships shown in Figs. 4 and 5 are sensitive to changes in μ. However, for the purposes of attenuation correction outlined in section 6, these effects are small.

The only difference between the calculations of K_{DP} and A_H for a given N_0, D_0 and μ, ignoring the constant terms, is that K_{DP} is proportional to the real part of the forward scatter amplitude whereas A_H is proportional to the imaginary part. Therefore any differences between the two parameters should become apparent when the scattering coefficients are studied closely. Figure 6 provides an explanation of the behaviour shown in Fig. 4. Once the raindrop size is larger than 3 mm the real part of the forward scatter amplitude increases less rapidly than the imaginary part. This means that there is more attenuation for a given phase shift for the larger drops, confirming the trend in Figs. 4 and 5. In physical terms, Fig. 4 suggests that the greatest amount of attenuation is caused by a small number of large drops being present within the radar volume. The implication follows that there are not simple linear relationships between attenuation and K_{DP}. Any method purporting to correct for total attenuation must have information on both the N_0 and D_0 of the rainfall spectrum causing the attenuation.

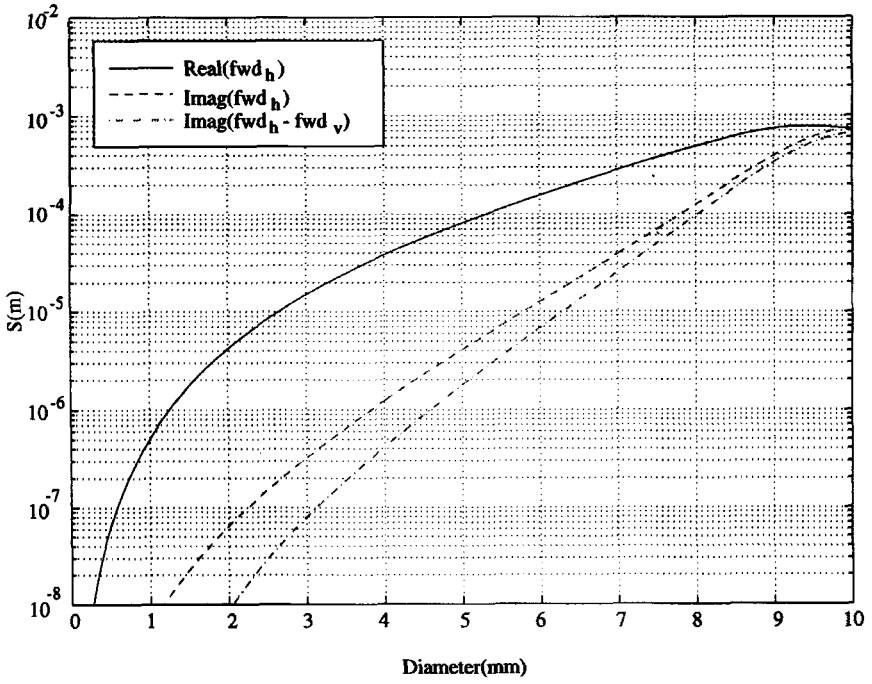

Figure 6. S-band variation of the forward scattering amplitude, S, (m) as a function of diameter, at 20 °C using Beard and Chuang (1987) shapes. See text for further explanation.

Attenuation is strongly dependent upon temperature (Jameson 1992), this is because the attenuation rate is controlled by molecular absorption and scatter out of the beam. Molecular absorption (the imaginary component) is enhanced at lower temperatures, and is dominant at the frequencies of 3 and 5 GHz over almost all raindrop sizes. This is shown in Fig. 7. At 20 °C the value of $\mathrm{Im}(S_{fH})$ is 40% less than when the temperature is 0 °C over a large range of the raindrop sizes. This implies that when using model results to correct for attenuation, great care must be taken in selecting a representative temperature for the raindrops.

6. Correction Scheme

The attenuation correction algorithm proposed in this paper which uses the two propagation observables, K_{DP} and the total amount of A_{H-V}, is outlined in Fig. 8. The total amount of A_{H-V} is estimated from the negative Z_{DR} beyond the intense precipitation, and is partitioned amongst the gates where $K_{DP} > 1^\circ$ km^{-1} with a weighting proportional to the magnitude of K_{DP}. Values of N_0 and D_0 are derived from A_{H-V} and K_{DP} (as in Fig. 5) at each gate, and A_H is computed at that gate. The corrected values of Z_H and Z_{DR} are then found from A_H and A_{H-V} at each gate. The highest values of attenuation occur in the regions of low N_0 and high D_0, and are only slightly affected by changes in the assumed value of μ.

The values of N_0 and D_0 are uniquely defined in K_{DP}/A_{H-V} space, if the value of μ in the DSD is predetermined, and the value of A_H can be computed at each gate. There are small errors in estimating A_H in this manner because the lines of constant N_0 and D_0

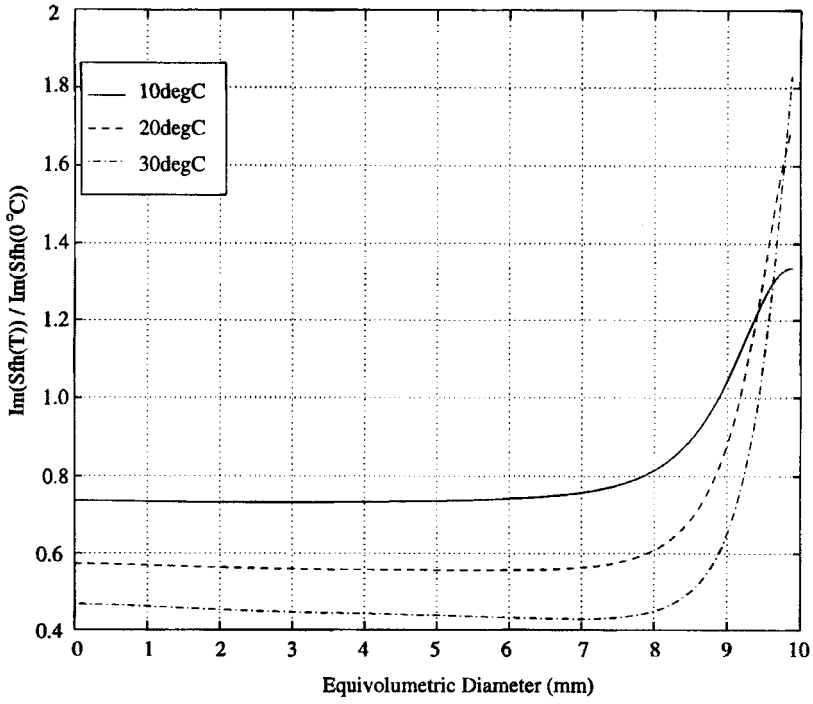

Figure 7. The variation of the forward scatter coefficient, $\mathrm{Im}(S_{fH})$, with temperature, T, and equivolumetric diameter at S-band using Beard and Chuang (1987) shapes and the dielectric constant of water. See text for further explanation.

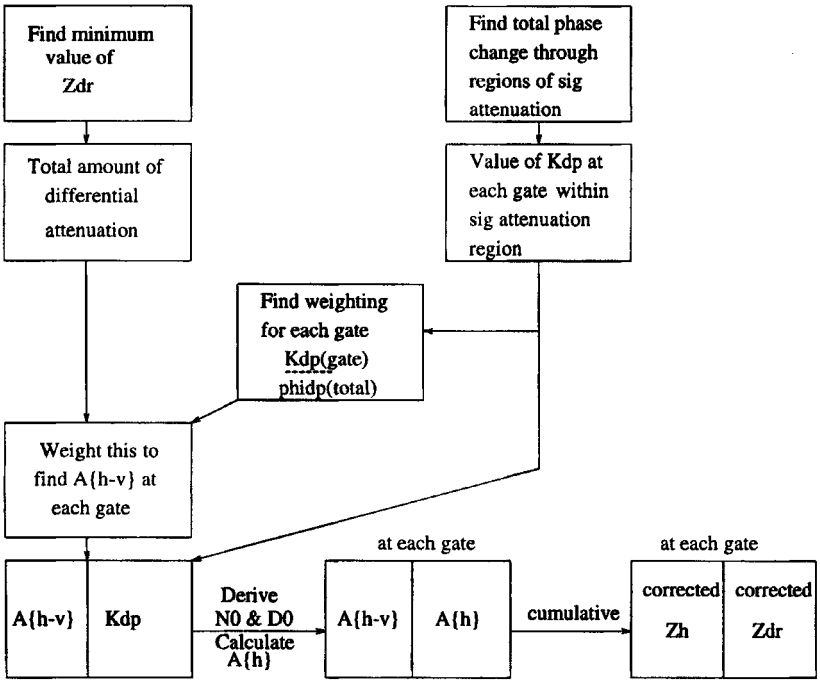

Figure 8. Flow diagram of the attenuation correction scheme. Criterion: Significant attenuation occurs in gate where uncorrected $Z_H > 30$ dBZ and $K_{DP} > 1^\circ$ km^{-1}. See text for further details.

TABLE 1. S-BAND VARIATION OF A_H, N_0 AND D_0 FOR A FIXED VALUE OF A_{H-V} (0.25 dB km^{-1}) AND VARIABLE K_{DP} AT 20 °C FOR $\mu = 0$.

K_{DP}(° km^{-1})	A_H(dB km^{-1})	N_0(m^{-3} mm^{-1})	D_0(mm)
11	0.34	600	4.00
13	0.35	1050	3.73
15	0.37	1660	3.53
17	0.39	2440	3.37
19	0.41	3420	3.24

For consistency see Figs. 4 and 5.

TABLE 2. AS TABLE 1 BUT FOR $\mu = 2$.

K_{DP}(° km^{-1})	A_H(dB km^{-1})	N_0(m^{-3} mm^{-1})	D_0(mm)
11	0.34	165	4.61
13	0.35	270	4.34
15	0.37	410	4.14
17	0.38	580	3.98
19	0.40	790	3.85

are almost parallel in K_{DP}/A_{H-V} space, as shown in Fig. 5 for $D_0 < 7$ mm. This means that for a fixed value of A_{H-V} and allowing K_{DP} to vary (to simulate random errors in the measurement of ϕ_{DP}), changes in D_0 are compensated for by changes in N_0. Table 1 highlights this point for a fixed A_{H-V} of 0.25 dB km^{-1}. For example, if the value of K_{DP} is $15 \pm 2°$ km^{-1} (realistic measurement error), then the associated value of A_H for a fixed $A_{H-V} = 0.25$ dB km^{-1} is 0.37 ± 0.04 dB km^{-1}. In other words, a 14% error in the measurement of K_{DP} will lead to a 11% error in the estimated value of A_H. If the total attenuation suffered by the beam is of the order of 5 dB, to have corrected Z_H to within 0.5 dB is more than satisfactory as it corresponds to an accuracy of derived rainfall rate of better than 10%.

Once the individual gate's value of A_H and A_{H-V} are known, the corrected values of Z_H and Z_{DR} can be extracted by cumulatively summing the attenuation parameters. This scheme is not numerically unstable, as any error at a particular gate does not contribute to successive gates, unlike iterative gate-by-gate methods. It is also physically based, the measured parameters being used to compute components of the DSD rather than relying upon a mathematical compensation effect as in the scheme of Tan and Goddard (1997). The scheme is also insensitive to hail which should not contribute to A_{H-V} or K_{DP}. However, within the scheme there are flaws. For each particular attenuation event A_{H-V} is divided between the gates depending upon the K_{DP} weighting, thus the attenuation corrected points are constrained upon a line of constant D_0, the coincidental values of N_0 being allowed to vary. This is easier to envisage with the aid of Fig. 5. D_0 is, in effect, defined over the whole precipitation core responsible for the attenuation, rather than allowing for any gate-to-gate variation which is possible within heavy storms over short spatial scales.

Comparing Tables 1 and 2 shows that the scheme is insensitive to μ variation for the purposes of calculating A_H from the K_{DP}, A_{H-V} pair. There appears to be a compensation effect between D_0 and N_0, with the result that there is only a 2.5% difference between the A_H calculated using $\mu = 0$ and that using $\mu = 2$. A fixed value of μ can therefore be used within the scheme.

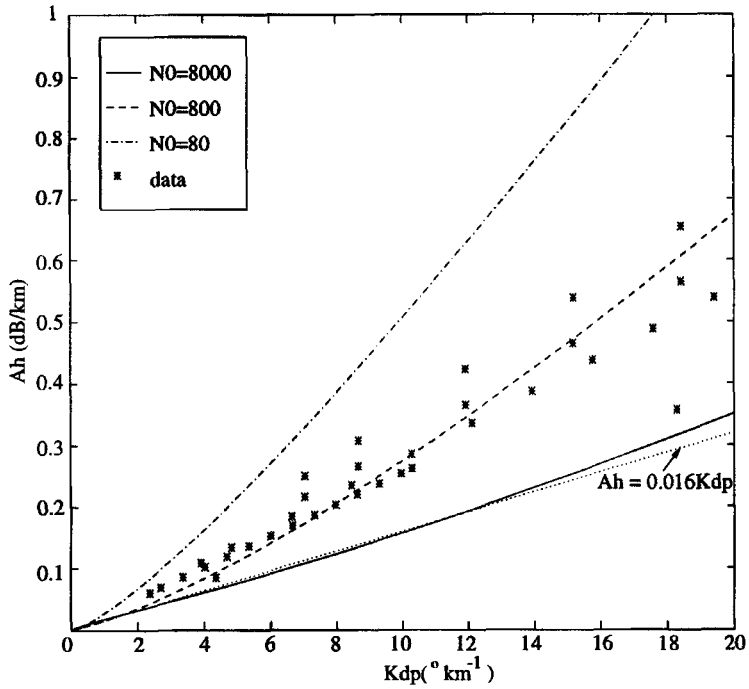

Figure 9. Attenuation, A_H, as a function of propagation, K_{DP}, for $\mu = 0$ at 20 °C. The data points are taken from several scans on 7 June 1996 as part of the correction scheme. See text for further details.

Figure 9 shows that most of the data points lie along the line of $N_0 = 800$ m^{-3} mm^{-1} with a D_0 of between 2.5 and 5 mm. The maximum value of D_0 used in the calculations of Bringi *et al.* was 2.5 mm. These results show that larger values of D_0 need to be considered and that the drop size spectrum should include raindrops of diameters up to 8 or 10 mm. There is a considerable departure from the $A_H = 0.016K_{DP}$ line in Fig. 9, which suggests that a different linear relationship exists for each value of D_0; this is consistent with the theoretical scattering calculations presented in Figs. 4 and 5. In short, the precise composition of the DSD has a large bearing upon the relationship between K_{DP} and the attenuation parameters, especially when it comprises a low concentration of large drops, and this is the advantage of implementing the attenuation algorithm detailed above. The scheme essentially defines an N_0, D_0 pair for a fixed value of μ in K_{DP}/A_{H-V} (A_H) space, and therefore is an improvement upon simply relating K_{DP} to the attenuation parameters with no knowledge of the DSD. We have assumed that at S-band δ is negligible. In operational terms the scheme assigns a value of D_0 to an entire rain shaft, thus fixing a linear relationship between K_{DP} and A_{H-V} which is unique to that particular core. The value of N_0 is not constrained and is allowed gate-to-gate variability through the rain shaft.

The values of total differential phase shift, ϕ_{DP}, at S-band when there is attenuation occurring, are quite large. Goddard *et al.* (1994) propose a method of self-calibration of Z_H to within 0.5 dB using the consistency of Z_H, Z_{DR} and K_{DP} in rain. This method has been used to calibrate Z_H for the data in this study. It relies on the fact that K_{DP}/Z_H as a function of Z_{DR} is virtually independent of μ in the DSD. The technique involves adjusting the Z_H calibration until the ϕ_{DP} calculated from the measured Z_H and Z_{DR} agrees with that observed. Provided the ϕ_{DP} used for calibration is limited to 30°, attenuation of Z_H and Z_{DR} is negligible and the method is reliable.

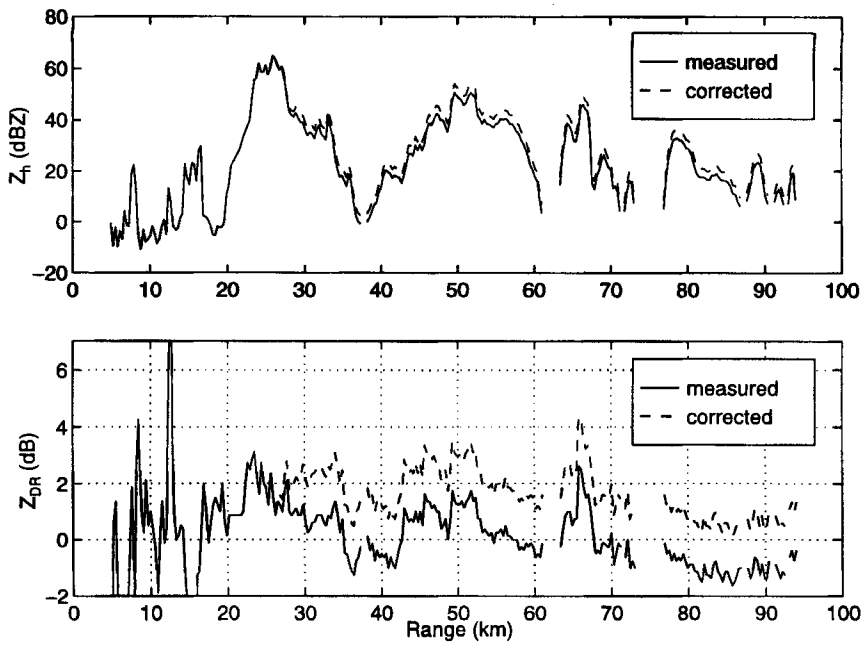

Figure 10. Fields along a ray showing the measured and attenuation corrected horizontally polarized backscatter reflectivity, Z_H, and differential reflectivity, Z_{DR}. Azimuth 269.6° at 19:36 GMT; gauge 7 is at a range of 32.2 km.

7. Results and validation

Figure 10 shows the fields of Z_H and Z_{DR} along the azimuth containing gauge 7 (see Fig. 2), which is situated at a range of 32.2 km. The measured Z_{DR} shows negative values at the back of the storm of -1.5 dB, implying that the total amount of A_{H-V} through the storm is 1.5 dB. The total amount of A_H is impossible to ascertain by simple inspection, it can only be obtained by calculation. The attenuation is occurring over three major precipitation cores centres at 25, 50 and 65 km from Chilbolton, with the greatest amount $\sim$1 dB occurring at the closest precipitation shaft where the temperature is about 20 °C (the temperature in Figs. 4 and 5). The correction to Z_{DR} has, by definition, removed the negative values in the region of light precipitation (the negative values of Z_{DR} between the radar and 20 km are caused by ground clutter). It is the corrected Z_H, Z_{DR} pair values at each gate which are important for rainfall rate estimation. Only if both components are accurately corrected will the rainfall rate estimate be meaningful; this can be tested by using *in situ* raingauges and statistical methods.

(*a*) *Raingauge*

Over a single ray, validation using a raingauge can be beneficial, although raingauge/radar comparisons are fraught with difficulties, such as point representivity, beam overshoot and precipitation wind-drift. The correction algorithm can also only be truly validated if the raingauge is situated in a region affected by attenuation, and if the gauge has a rapid response time, because attenuation events are transitory. Gauge 7 was positioned in such a place at 1936 UTC; gauge 5 was between the radar and gauge 7, in the region causing the attenuation. Figure 11 shows the rainfall rate traces of gauges 5 and 7. Gauge 5 was recording 267 mm hr^{-1} at the time of the coincidental plan position indicator (PPI)

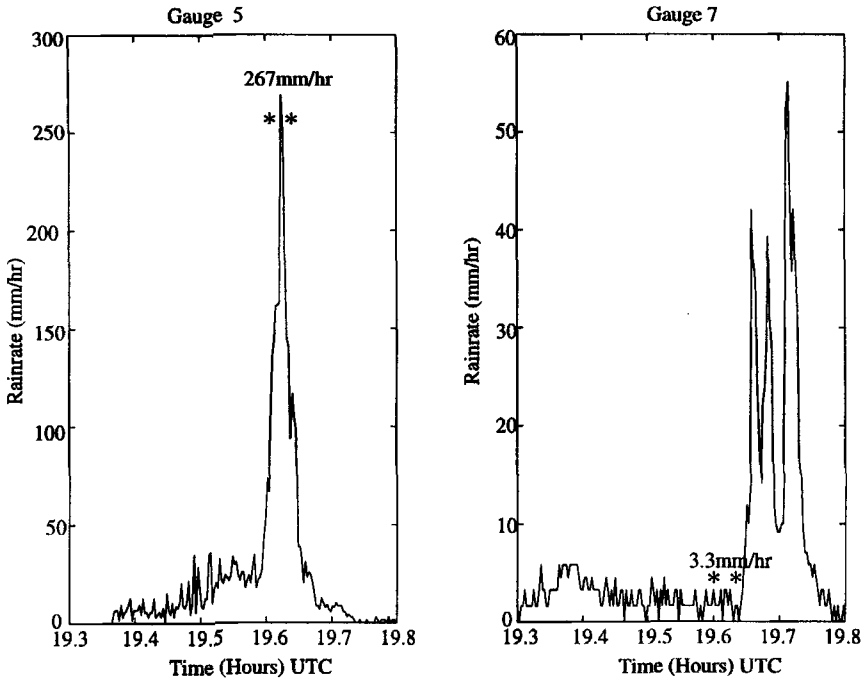

Figure 11. Rainfall rates at gauges 5 and 7 during the time of the PPI shown in Fig. 2. The stars delimit the start and finish time of the PPI scan; the time resolution of the gauges is 10 seconds.

scan; this was very close to the radar estimated R (assuming that hail was not present in the precipitation volume), using both Z_H (=58 dBZ) and Z_{DR} (=2.6 dB) (DSD spectrum truncated at 10 mm), of 268 mm hr^{-1}, although it must be emphasised that at such high reflectivities the estimation of R is very dependent upon the value of μ used within the DSD. There is evidence from the radar scan that hail is present in the immediate vicinity of gauge 5, resulting in spurious R estimations using Z_H and Z_{DR}. Regions of hail tend to give the radar signature of high Z_H and low values of Z_{DR} (Aydin *et al.* 1986), if the hail is tumbling i.e. appears to be anisotropic to the polarization radar. If the radar signature is interpreted as being due to rain in these high Z_H low Z_{DR} regions the rain DSD equivalent is a high number concentration of small raindrops. As rainfall rate is a volumetric effect then the result is a seemingly large value of R.

Using the uncorrected values of Z_H and Z_{DR} over the position of gauge 7 gives an estimated R of 10 mm hr^{-1} (using $\mu = 0$), whereas the corrected value of R is 3.0 mm hr^{-1}. There is a seeming paradox here, in that the estimated rainfall rate has been reduced by correcting for attenuation. The reason for this is that the value of Z_{DR} has been increased, which effectively reduces the number of small raindrops within the volume. This effect would not have occurred if R had been estimated using Z_H alone; the corrected and uncorrected values would have been 7.5 mm hr^{-1} and 4.7 mm hr^{-1} respectively. The corrected value of R (3.0 mm hr^{-1}) is within 10% of the gauge 7 recorded rainfall rate of 3.3 mm hr^{-1}. On these results the attenuation correction algorithm appears to be effective.

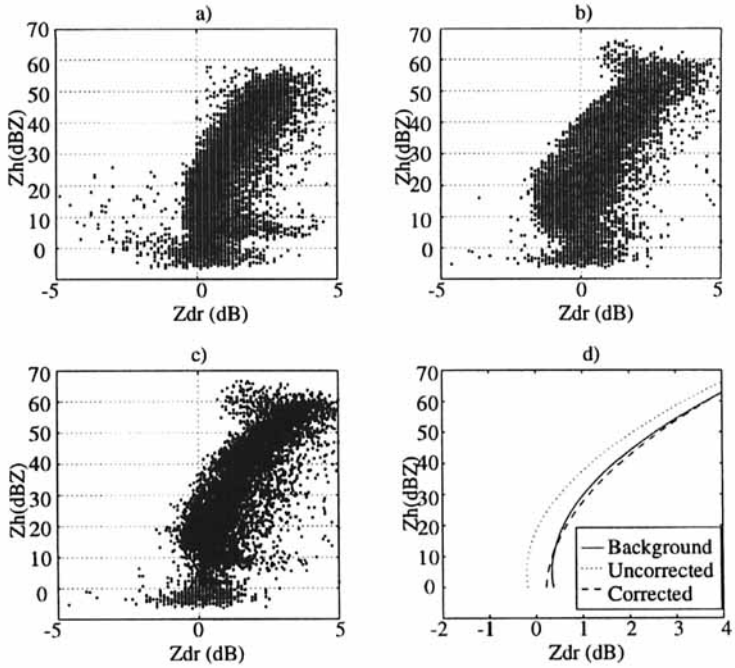

Figure 12. Horizontally polarized backscatter reflectivity, Z_H, against differential reflectivity, Z_{DR}, scatterplots showing (a) 'background' unattenuated azimuths, (b) uncorrected attenuated azimuths, (c) attenuated azimuths following attenuation correction and (d) comparison between the polynomial fits for the scatterplots. All for the plan position indicator shown in Fig. 2.

(*b*) *Statistical*

Using gauges to validate attenuation correction schemes has a limited scope, especially where rain gauges are sparsely distributed. A better means of validation would be to check for internal 'self consistency' within the scan. That is to compare regions affected by attenuation with those that are not, in terms of Z_H and Z_{DR}. The scatterplots in Fig. 12 show remarkable detail as to the efficacy of the attenuation algorithm. The feature to note is the 'bulge' of negative Z_{DR} in (b) which indicates the need for attenuation correction. This is most pronounced between 10 and 25 dBZ, and for the correction algorithm to be judged successful these negative values must not only be removed, but they must be adequately redistributed such that the corresponding values of Z_H are reasonable. An attenuated azimuth is defined as a ray which contains negative Z_{DR} (outside of the clutter region), and it includes the unattenuated portions of the ray between the radar and the attenuating core. Qualitatively comparing Fig. 12(a) and (c), that is the background (azimuths unaffected by attenuation) and corrected azimuths respectively, shows that the scheme does successfully correct for attenuation. The majority of the negative Z_{DR} has been removed, all that remains is due to clutter similar to the pattern in (a). An interesting feature to note in Fig. 12(b) and (c) is the pairs of high Z_H (>55 dBZ) and low Z_{DR} (<2 dB), possibly being caused by hail. However it is only upon inspection of the scatterplot polynomials in Fig. 12(d) that the scheme can truly be shown to correct to a high degree of accuracy in the cases examined, for both Z_H and Z_{DR}; this being the vital factor for rainfall rate estimation. The corrected polynomial results in a curve similar in shape and form to the background fit. The coefficients of the second-order polynomial fits provide a more quantitative compar-

TABLE 3. COEFFICIENTS OF THE SECOND-ORDER POLYNOMIAL FITS SHOWN IN FIG. 12(d) FOR Z_{DR} AS A FUNCTION OF Z_H.

Data set	α_0	α_1	α_2
Background	0.0011	−0.0112	0.3701
Uncorrected	0.0011	−0.0098	−0.1812
Corrected	0.0009	0.0036	0.2214

ison between the separate data sets, shown in Table 3, the form of the polynomial being $\alpha_0 Z_H^2 + \alpha_1 Z_H + \alpha_2$. Table 3 shows that all three curves are very similar in shape (the α_0 and α_1 terms), which is the result expected upon inspection of Fig. 12. The most important difference between the curves occurs in the constant α_2 term, which physically moves the fit to higher or lower values of Z_{DR} for a constant Z_H. The corrected data-set constant term gives the closest match to the background value; the uncorrected α_2 is negative, this being indicative of the effects of attenuation. An exact match is not expected because of natural variation in the DSD throughout the PPI.

8. IMPLICATIONS FOR ATTENUATION CORRECTION AT C-BAND

Attenuation by rainfall is much larger at C-band than at S-band and, because most European and Japanese operational networks use C-band, the need for a method of correcting for attenuation at C-band is much more pressing. As a first step to exploring how the K_{DP}/A_{H-V} S-band algorithm would function at C-band, Fig. 13 displays the relative contribution of different raindrop sizes to the various forward-scattering amplitudes for a Marshall and Palmer (1948) DSD with a rainfall rate of 100 mm hr^{-1}. If the curves were identically shaped then a single relationship would link K_{DP} with A_H as proposed by Bringi *et al.* (1990). At C-band the position of the peaks of the three curves are less consistent than at S-band; the K_{DP} curves are similar for the two wavelengths, but the attenuation is weighted more towards larger drops at C-band compared with S-band. However, for drops larger than 6 mm the shapes of the C-band curves are more consistent. The sensitivity to μ, the index in the gamma function, is far lower at C-band, as demonstrated by Fig. 14, showing that the A_H versus A_{H-V} curves for $\mu = 0$ and $\mu = 5$ are almost identical at C-band.

Ideally C-band polarization data should be used to assess the efficiency of the proposed correction scheme. Such data are not available to us, so our first step in assessing the efficiency of the correction algorithm at C-band was to use the S-band data to simulate attenuated C-band data. This was achieved by taking a ray of attenuated S-band data to ensure that appreciable attenuation is observed at C-band. The S-band data were first corrected for attenuation using the method outlined in section 6. S-band values of Z_H and Z_{DR} at each gate were then converted to C-band values, assuming the precipitation was rain; this involves calculating N_0 and D_0 at each gate using the standard technique of Seliga and Bringi (1976). If hail contaminates Z_H and Z_{DR} these N_0 and D_0 values will be spurious, but because both C- and S-band will both be contaminated, the C-band Z_H and Z_{DR} should be adequately simulated for our purpose.

However, in order to simulate the values of A_H, K_{DP} and δ at C-band, only the regions where there was appreciable attenuation at S-band were used. The N_0 and D_0 values derived from the observed A_{H-V}, K_{DP} at S-band were used to calculate these C-band parameters.

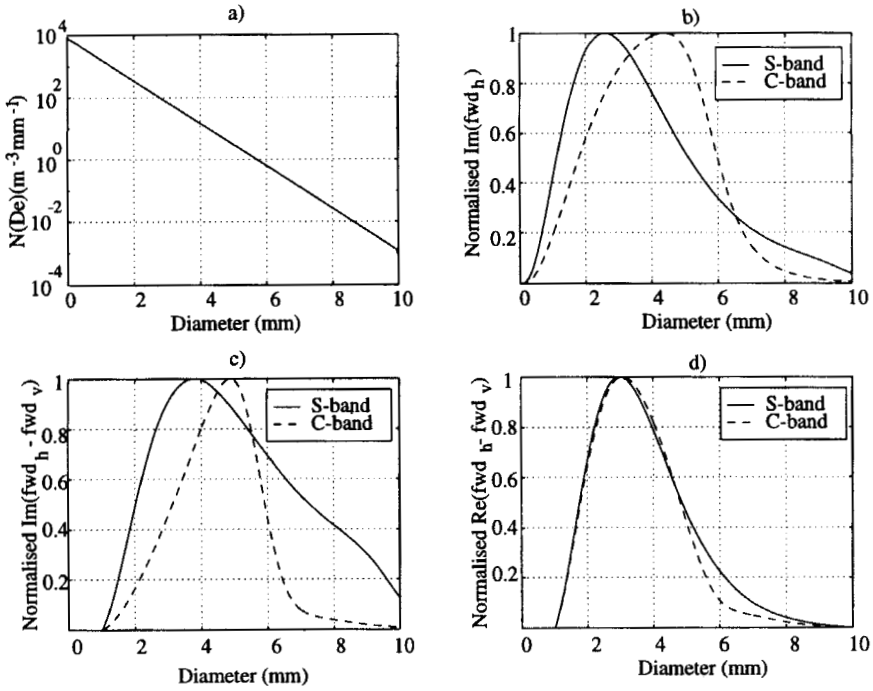

Figure 13. (a) Marshall and Palmer (1948) drop size distribution, DSD, for a rainfall rate of 100 mm hr^{-1}; (b) Normalised imaginary part of the forward-scatter matrix in the horizontal at S- and C-band (indicative of A_H), weighted by the DSD shown in (a); (c) as (b) except indicative of A_{H-V}; (d) as (b) except indicative of K_{DP}. All at 0 °C and R = 100 mm hr^{-1} and values normalised by dividing by the maximum of the function. See text for further details.

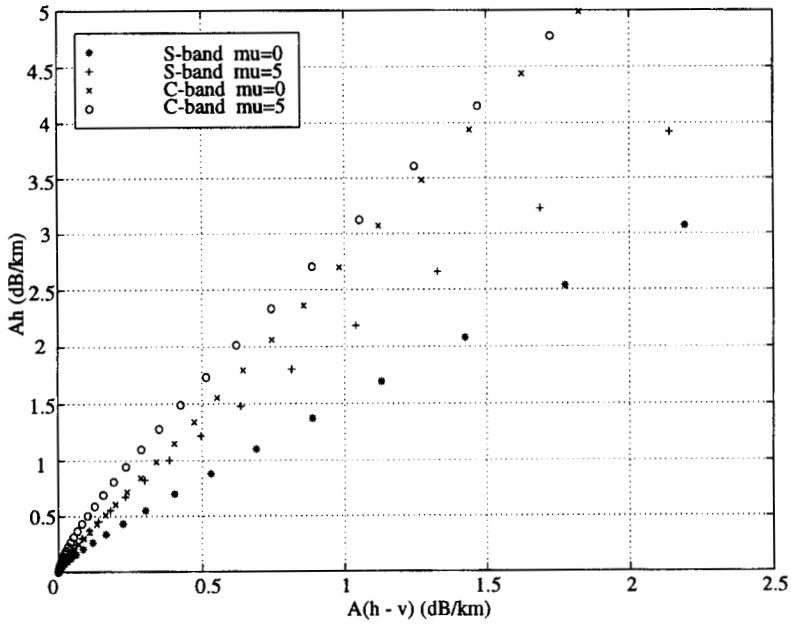

Figure 14. S-band and C-band A_H as a function of A_{H-V} at 20 °C for $\mu = 0$ and $\mu = 5$ in a normalised gamma drop size distribution. $N_0 = 8000$ m^{-3} mm^{-1}. See text for further details.

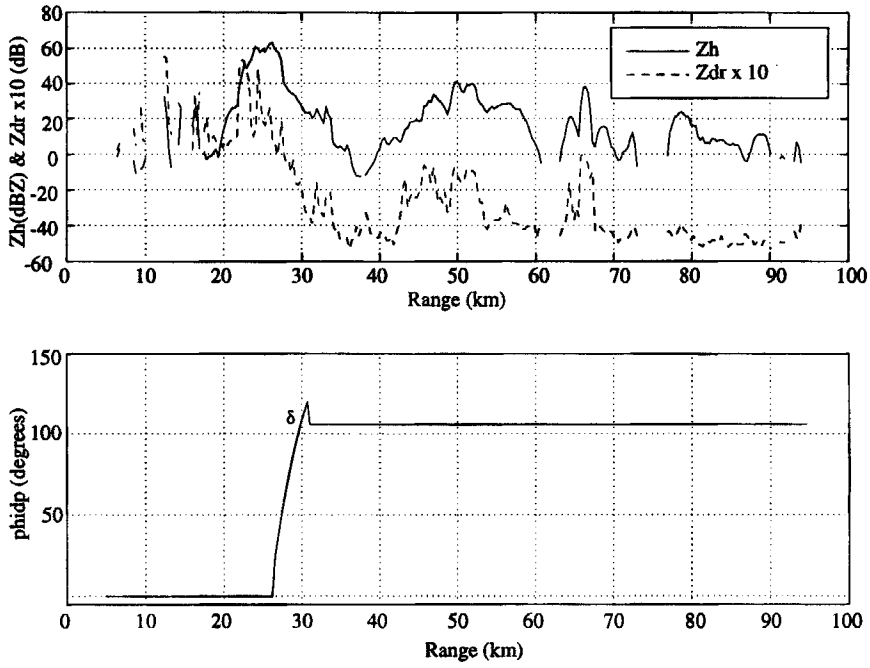

Figure 15. Ray along azimuth 268.9° showing the attenuated values of Z_H and Z_{DR} and the ϕ_{DP} data simulated at C-band. See text for further details.

This should ensure that the calculated attenuation is only due to the rain component of the precipitation.

The predicted C-band data for the S-band data in Fig. 10 are displayed in Fig. 15. The Z_{DR} behind the intense region of precipitation has reached −5 dB, which indicates that throughout the ray 5 dB of differential attenuation has occurred (cf. 20 dB of A_H). This compares with 1.5 dB for the equivalent S-band ray shown in Fig. 10. Using the linear relationships proposed by Bringi *et al.* (1990) to act as a rough guide, A_{H-V} at C-band should be a factor of four greater than at S-band. This implies that the values of negative C-band Z_{DR} are of the correct order of magnitude.

The stimulated C-band ϕ_{DP} data show a change of greater than 100° over a range of 4 km. Another feature of note is the transient spike of δ occurring at a range of 30 km which has a magnitude of $\sim +15°$. Throughout the large differential phase shift region δ contributes to ϕ_{DP}, it is only when the beam emerges from the intense precipitation core that the characteristic spike is observable. In practice ϕ_{DP} ray profiles at C-band tend to be noisier than this (Bringi *et al.* 1991).

There are difficulties in adjusting the scheme to cope with the addition of δ, the largest problems occurring at the gates where the ray enters and subsequently emerges from the high D_0 rain shaft. (In the simulated dates shown in Fig. 15, δ adds a constant offset to ϕ_{DP}; this is due to the value of D_0 being prescribed for the whole attenuating region by the scheme, which is perhaps unrealistic.) K_{DP} at these gates is therefore spurious and, as a consequence, the weightings calculated using the value of K_{DP} are incorrect throughout the attenuating rain shaft. The use of K_{DP} and A_{H-V} to calculate A_H are also compromised; the result being that A_H is hugely overestimated. The scheme, therefore, needs to be modified to cope with the significant contribution from δ.

As there is a significant amount of random noise associated with the measurement of ϕ_{DP}, it is necessary to smooth the ϕ_{DP} parameter so that K_{DP} can be extracted. Within

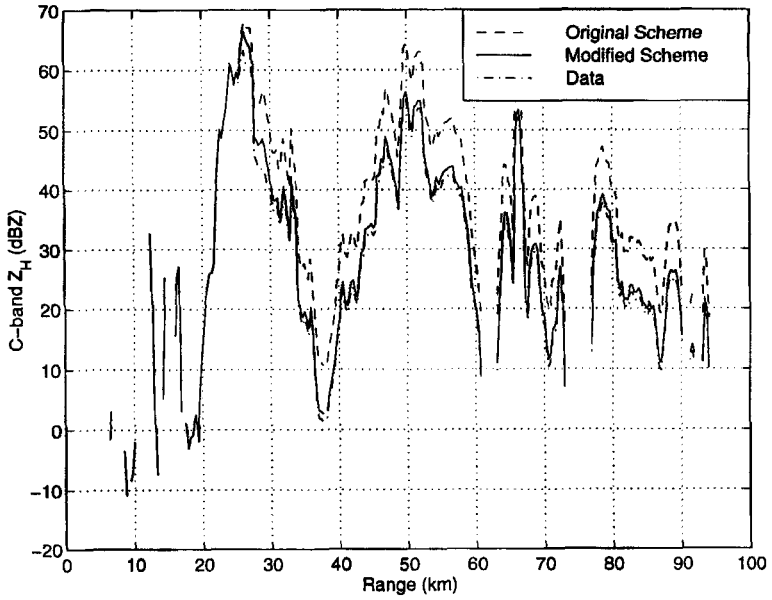

Figure 16. Comparison between the original attenuation correction scheme proposed by this work (dashed), the modified scheme which uses a look-up table for A_H (solid) and the unattenuated data (dash-dot). The data are along the same azimuth shown in Fig. 15, at C-band. See text for further details.

the attenuation correction code a fourth-order Butterworth filter (Parks and Burns 1987) is utilized for this purpose, using a sampling rate of one tenth the original data. This filter can smooth out the jump in ϕ_{DP} at the entry and emergent range gates, and is also effective when a δ spike is present over a limited number of gates. This allows the weightings to be correctly assigned, but the actual values of K_{DP}, and hence the calculated values of A_H, are incorrect in this case where δ is adding a constant offset to ϕ_{DP}.

The attenuation correction algorithm, therefore, needs to be modified for use at C-band. The step involving the weightings can still be used, but an alternative to using K_{DP} and A_{H-V} to calculate N_0 and D_0, and hence A_H, needs to be found.

The algorithm can be modified to accommodate the determination of A_H when the K_{DP} signal is contaminated by δ by using a look-up table to derive the A_H from A_{H-V}. (Figure 6 suggests that there are not the problems in relating the two attenuation parameters to one another that there are in relating them to K_{DP}. The relationship between A_H and A_{H-V} should be relatively independent of N_0.)

Figure 14 shows that there is a dependency upon the value of μ in the DSD; the differences may not appear to be large but, as they add cumulatively along a ray, then an error of 0.2 dB km^{-1} could result in an overall error in the estimation of Z_H of 2 dBZ over a 10 km precipitation path length at C-band, and would clearly be worse for very extensive echoes. This error is quite small, though, when compared with the difference between the unattenuated C-band data and the corrected fields, shown in Fig. 16.

At this point a definition of terms is required. The *unattenuated* data relate to the C-band ray directly calculated from the corrected S-band Z_H and Z_{DR}; these are used as 'truth' against which to test the attenuation correction schemes. The *attenuated* data relate to the same ray but with the calculated A_H and A_{H-V} subtracted from Z_H and Z_{DR} respectively; it is this ray which is used as the input to the C-band correction scheme. The *attenuation corrected* data are the output from the correction scheme.

The scheme, run without the modification to account for δ (dashed line in Fig. 16), shows an overestimation of 8 dBZ in the Z_H field. This will lead to a serious overestimation of the rainfall rate in the regions behind the precipitation core which is causing the attenuation. When the look-up table modification is included, the algorithm gives values of Z_H to within 1 dBZ of the unattenuated data, although there is a difference of $\sim$1 dB within the precipitation core suggesting that the distribution of the correction is not altogether accurate within this region.

If it is correct to assume that at C-band A_H and A_{H-V} are linearly related then the C-band algorithm could be quite simple. The values of total attenuation could be derived from the differential attenuation (i.e. negative Z_{DR}) observed behind the intense precipitation. This relies on the insensitivity of the $A_H - A_{H-V}$ relationship to changes in μ (Fig. 14).

In addition we note that the most severe cases of attenuation result from heavy rain having exceptionally large sized drops. Figure 9 shows that the values of D_0 are 3 or 4 mm, and lie along the curve for $N_0 = 800$ m^{-3} mm^{-1}. Comparison of Figs. 4 and 5 shows that for this value of N_0 the differential attenuation is about 75% of the horizontal attenuation. This suggests that if only one polarization is available for an operational radar then the vertical polarization would be preferable, because the attenuation would only be about one third of the value for horizontal polarization. The UKMO currently uses vertical polarization (Fair *et al.* 1990) but, as far as we can ascertain, is alone in this. Presumably horizontal polarization has generally been chosen because there is slightly less ground clutter for this polarization, as demonstrated by its predominantly negative values of differential reflectivity (Hall *et al.* 1984).

9. Conclusions

Previously, attenuation correction schemes have relied upon gate-by-gate iterative methods which quickly become unstable. These methods also rely upon backscatter parameters, such as Z_H and Z_{DR}, which can become contaminated with hail within the volume. Hail is indistinguishable from rain when single parameter radar is used but should produce much less attenuation because of its low concentration. Therefore when hail is present the correction schemes may be needlessly implemented, resulting in overcorrection.

A new attenuation correction algorithm has been developed which makes use of the total amount of A_{H-V} at the back of the storm, determined by the magnitude of the negative Z_{DR} in the regions of light precipitation, and the measured ϕ_{DP}. The scheme has been implemented at S-band and, using raingauge and statistical validation, found to accurately correct for attenuation. In this work it was assumed that the rain causing the attenuation was at 20 °C. Generally, because attenuation is temperature dependent, different look-up tables need to be generated for different temperatures. The advantages of the scheme are that it is numerically stable and relatively insensitive to hail. Simpler methods using K_{DP} alone do not provide a unique solution. Ryzhkov and Zrnić (1994) observed a differential attenuation which was twice as much as that predicted from K_{DP} by Bringi *et al.* (1990), and suggested that this was due to half-melted ice cores. The calculations and observation suggest that this higher attenuation for a given K_{DP} is due to the larger raindrops, and that Bringi *et al.* (1990) underestimated the attenuation by limiting the maximum value of D_0 to 2.5 mm.

Implementation of the combined ϕ_{DP} Z_{DR} technique at C-band is more difficult, because at this shorter wavelength there is more differential phase shift on backscatter by the large oblate raindrops. This backscatter phase shift is a transient superposed on the propagation phase, and makes the propagation component more difficult to estimate. However it

seems that a C-band the differential attenuation is more closely related to the total attenuation than at S-band. This suggests that a simpler algorithm may be implemented, in which the total attenuation is simply related to the total differential attenuation which is found from the magnitude of the negative Z_{DR} in low intensity precipitation regions at greater range. It is suggested by these studies that this algorithm is not temperature dependent, because the ratio of total to differential attenuation varies little with temperature. Further work is needed to confirm this suggestion.

The implementation of polarization diversity involves the installation of a fast switch, so that pulses can be transmitted alternately with horizontal and vertical polarization. The implications for dwell time and scanning rates are discussed in Sachidananda and Zrnić (1985). In all these attenuation algorithms it is assumed that the radar beam is sampling at levels below the zero degree isotherm, and is in the rain or hail rather than the ice above the melting layer. Since nearly all severely attenuating storms occur in the summer this should not be too severe a restriction, but clearly it does place a limit on the absolute maximum range for the technique. Finally we note that if polarization diversity is not available, then it is preferable to use vertical polarization, as the attenuation is much reduced compared with that occurring in the horizontal.

Acknowledgements

This work was supported by the Natural Environmental Research Council 'HYREX' grant GST/02/718. We thank the Radio Communications Research Unit group at Rutherford Appleton Laboratory for allowing access to the Chilbolton radar. Jothiram Vivekenanden (National Center for Atmospheric Research) provided the scattering code.

References

Atlas, D., Harper, W. G., Ludlam, F. H. and Macklin, W. C. 1960 Radar scatter by large hail. *Q. J. R. Meteorol. Soc.*, **86,** 468–482

Aydin, K., Seliga, T. and Balaji, V. 1986 Remote sensing of hail with a dual linear polarisation radar. *J. Clim. Appl. Meteorol.*, **25,** 1475–1484

Aydin, K., Zhao, Y. and Seliga, T. A. 1989 Rain-induced attenuation effects on C-band dual-polarisation meteorological radars. *IEEE Trans. Geosci. Remote Sens.*, **27,** 57–65

Beard, K. V. and Chuang, C. 1987 A new model for the equilibrium shape of raindrops. *J. Atmos. Sci.*, **44,** 1509–1524

Blackman, T. M. 1996 'Observations and interpretations of differential phase shift in precipitation using S- and K_A-band radars'. PhD Thesis, UMIST

Bringi, V. N., Chandrasekar, V., Balakrishnan, N. and Zrnić, D. S. 1990 An examination of propagation effects in rainfall on radar measurements at microwave frequencies. *J. Atmos. Oceanic Technol.*, **7,** 829–840

Bringi, V. N., Chandrasekar, V., Meischner, P., Hubbert, J. and Golestani, Y. 1991 Polarimetric radar signature of precipitation at S- and C-bands. *IEEE Proc F*, **138,** 109–119

Caylor, I. J. 1989 'Radar observations of maritime clouds using dual linear polarisation'. PhD Thesis, UMIST

Cheng, L. and English, M. 1983 A relationship between hailstone concentration and size. *J. Atmos. Sci.*, **40,** 204–213

Collier, C. G. 1990 Radar data processing and short-period forecasting in the United Kingdom. P. 599 in *Radar in meteorology*. First edition. Ed. D. Atlas. American Meteorological Society, Boston

Delrieu, G., Creutin, J. D. and Saint-Andre, I. 1991 Mean K-R relationships: Practical results for typical weather radar wavelengths. *J. Atmos. Oceanic Technol.*, **8,** 467–476

Delrieu, G., Caoudal, S. and Creutin, J. D. 1997 Feasibility of using mountain return for the correction of ground-based X-band weather radar data. *J. Atmos. Oceanic Technol.*, **14,** 368–385

Fair, C. A., James, P. K. and Larke, P. 1990 The United Kingdom weather radar network. Pp. 147–154 in *Cost 73: Weather radar networking*. Eur 12414 EN-ER. Kluwer, Dordrecht, The Netherlands

Goddard, J. W. F., Tan, J. and Thurai, M. 1994 Technique for calibration of meteorological radar using differential phase. *Electron. Lett.*, **30,** 166–167

Green, A. W. 1975 An approximation for the shape of large raindrops. *J. Appl. Meteorol.*, **14,** 1578–1583

Gunn, K. L. S. and East, T. W. R. 1954 The microwave properties of precipitation particles. *Q. J. R. Meteorol. Soc.*, **80,** 522–545

Hall, M. P. M., Goddard, J. W. F. and Cherry, S. M. 1984 Identification of hydrometeors and other targets by dual-polarisation radar. *Radio Sci.*, **19,** 132–140

Hildebrand, P. H. 1978 Iterative correction for attenuation of 5 cm radar in rain. *J. Appl. Meteorol.*, **17,** 508–514

Hitschfeld, W. and Bordan, J. 1954 Errors inherent in the radar measurement of rainfall at attenuating wavelengths. *J. Meteorol.*, **11,** 58–67

Illingworth, A. J. and Caylor, I. J. 1989 Polarisation radar estimates of raindrop size spectra and rainfall rates. *J. Atmos. Oceanic Technol.*, **6,** 939–949

Jameson, A. R. 1983 Microphysical interpretation of multi-parameter radar measurements in rain: Part I interpretation of polarisation measurements and estimation of raindrops shapes. *J. Atmos. Sci.*, **40,** 1792–1802

Jameson, A. R. 1992 The effect of temperature on attenuation-correction schemes in rain using polarization propagation differential phase shift. *J. Appl. Meteorol.*, **31,** 1106–1118

Kabeche, A. and Testud, J. 1995 Stereoradar meteorology: A new unified approach to process data from airborne or ground based meteorological radars. *J. Atmos. Oceanic Technol.*, **12,** 259–270

Liebe, H. J., Manabe, T. and Hufford, G. A. 1989 Millimeter-wave attenuation and delay rate due to clouds/fog conditions. *IEEE AP*, **37,** 1617–1623

Marshall, J. S. and Palmer, W. M. K. 1948 The distribution of raindrops with size. *J. Meteorol*, **6,** 243–248

McCormick, G. C., Allan, L. E. and Hendry, A. 1979 The backscatter matrix of ice samples: its relation to the identification of hail by radar. *J. Appl. Meteorol.*, **19,** 77–84

O'Brien, S. G. and Geodecke, G. H. 1988 Scattering of millimetre waves by snow crystals and equivalent homogeneous symmetric particles. *Appl. Opt.*, **27,** 2439–2444

Oguchi, T. 1973 Attenuation and phase rotation of radio waves due to rain: Calculations at 19.3 and 34.8 GHz. *Radio Sci.*, **8,** 31–38

Parks, T. W. and Burns, C. S. 1987 *Digital filter design*, John Wiley & Sons, Chichester, UK

Pruppacher, H. R. and Pitter, R. L. 1971 A semi-empirical determination of the shape of cloud and raindrops. *J. Atmos. Sci.*, **28,** 86–94

Ray, P. S. 1972 Broadband complex refractive indices of ice and water. *Appl. Opt.*, **11,** 1836–1844

Ryzhkov, A. V. and Zrnić, D. 1994 Precipitation observed in Oklahoma mesoscale convective systems with a polarimetric radar. *J. Appl. Meteorol.*, **33,** 455–464

Sachidananda, M. and Zrnić, D. 1985 Zdr measurement considerations for a fast scan capability radar. *Radio Sci.*, **20,** 907–922

1986 Differential propagation phase shift and rainfall estimation. *Radio Sci.*, **21,** 235–247

Scarchilli, G., Gorgucchi, E., Chandrasekar, V. and Seliga, T. A. 1993 Rainfall estimation using polarimetric techniques at C-band frequencies. *J. Appl. Meteorol.*, **32,** 1150–1160

Seliga, T. A. and Bringi, V. N. 1976 Potential use of radar differential reflectivity measurements at orthogonal polarisations for measuring precipitation. *J. Appl. Meteorol.*, **15,** 69–76

Tan, J. and Goddard, J. W. F. 1997 'The use of compensation effect in attenuation correction for C-band radars'. Pp. 29–30 in Proceedings of the 28th conference on radar meteorology, 7–12 Sept., Austin, Texas, USA

Ulbrich, C. W. 1983 Natural variations in the analytical form of the raindrop size distribution. *J. Clim. Appl. Meteorol.*, **22,** 1764–1775

Waterman, P. C. 1965 Matrix formulation of electromagnetic scattering. *Proc. IEEE*, **53,** 805–812

Wilson, D. R., Illingworth, A. J. and Blackman, T. M. 1997 Differential doppler velocity: A radar parameter for characterising hydrometeor size distributions. *J. Appl. Meteorol.*, **36,** 649–663